Journal of Solid Mechanics Vol. 14, No. 3 (2022) pp. 398-417
DOI: 10.22034/jsm.2022.1950821.1727

Research Paper

Deformation of Irregular Layered Half-Space Due to Long Strike Slip Fault

M. Malik [1], Savita [2,*], R. Kumar Sahrawat [2]

[1]*Department of Mathematics, All India Jat Heroes' Memorial College, Rohtak-124001, India*
[2]*Department of Mathematics, Deenbandhu Chhotu Ram University of Science and Technology, Murthal-131039, India*

Received 15 June 2022; accepted 15 August 2022

ABSTRACT

This paper investigates the effect of irregular boundary and source depth in a two dimensional model due to movement of a long strike slip fault. A model having horizontal orthotropic elastic layer of uniform thickness coupling in three different ways to an irregular boundary of an orthotropic elastic half-space (having rectangular shaped irregularity on its boundary surface) has been considered. To study the effect of fault depth, we divide the problem into two cases. In case first, the fault is assumed to be present in regular orthotropic elastic layer at a distance say $'d'$ from the upper surface of the layer. In second case, the fault is assumed to be present in irregular orthotropic elastic half-space at same depth $'d'$ from the boundary surface of elastic half-space. For each type of coupling, the effect of rectangular irregularity and variation in fault depth on displacements and stresses for both layers and half-space are studied graphically. The present paper has wide applications in material science engineering, geosciences and soil mechanics.

Keywords : Strike slip; Welded contact; Smooth-rigid contact; Rough-rigid contact; Rectangular irregularity.

1 INTRODUCTION

THE phenomenon of the earthquake in theoretical seismology developed with the help of mathematical methods in which anisotropy has been derelict in the studies of the earth's crust. It can be examined by accepting the fact that there is seismic anisotropy present in the earth's crust and mantle. The presence of anisotropic minerals such as olivine and orthopyroxenes results in seismic anisotropy in the earth's upper mantle. The study of impact of surface loads on the horizontally layered elastic anisotropic, specifically, orthotropic materials, has been creating abundant interest in the fields like, material sciences, geosciences and soil mechanics. Now days, the development of a composite laminated material, an assemblage of layers of composite materials which can be coupled to endow with required engineering properties and earthworks like fills or pavements, composed of horizontal layers of

*Corresponding author.
E-mail address: savitadhankhar67@gmail.com (Savita)

different materials is the need of hour. Moreover, natural deposits in the earth are also horizontally layered. The material at a point of a layer may have different elastic properties in different directions. It is documented that the upper part of the earth has an orthorhombic symmetry. When one of the planes of symmetry in an orthorhombic symmetry is horizontal, the symmetry is termed as orthotropic symmetry and the most symmetry systems in the earth crust also have orthotropic orientations (Crampin [1]). A material with three mutually perpendicular planes of elastic symmetry at a point is said to possess orthotropic symmetry which is exhibited by olivine and orthopyroxenes, the principal rock-forming minerals of the deep crust and upper mantle. The static deformation of a layered or semi-infinite orthotropic/isotropic elastic media due to strike slip and dip slip faults has been studied by many researchers, e.g. Singh and Rani [2], Rani and Singh [3], Garg et al. [4], Singh and Garg [5], Bonafede et al. [6], Arya et al. [7] etc. In geophysics, the interface between the earth's crust to a base may be any of three types; smooth-rigid, rough-rigid and perfectly welded. Some researchers like Garg and Sharma [8] obtained the displacements and stresses at any point of an elastic layer coupling differently (smooth-rigid, rough-rigid and perfectly welded) to a half-space due to a very long vertical strike slip fault and their variations with the horizontal distance from the fault. Madan and Garg [9] further investigated the results of Garg and Sharma [8] by replacing the elastic layer with an orthotropic elastic layer over a base due to a long inclined strike slip fault. Chugh et al. [10] obtained the deformation of orthotropic elastic layer coupling in three different ways to a regular homogeneous orthotropic elastic half-space due to a long blind strike slip fault and gave the generalization of the results for an isotropic medium. Malik and Singh [11] obtained the results for the displacements and stresses in a homogeneous perfectly elastic half-space caused by a buried strike slip line source by considering the rigid surface. The model, they considered is very useful when the medium is very hard on the other side of the material discontinuity and a volcanic edifice is composed of such layers at depths below. The problems of static and quasi-static deformation with irregular boundaries have gained much importance in geophysics due to their closeness to their natural environmental conditions. It leads to a better understanding and better predictions for the seismic behavior at continental margins and mountain roots. It is, therefore, interesting to study the static deformation in media with irregular boundaries. Many researchers have studied the problem of irregular boundaries. Selim [12] discussed the problem of a two-dimensional static deformation due to normal line-load acting inside an irregular initially stressed isotropic half-space and irregularity was of rectangular shape. Madan and Gaba [13] studied the effect of rectangular and parabolic irregularities present in an orthotropic elastic medium. The expressions for the displacements and shearing stresses in an orthotropic elastic layer over an irregular elastic half-space have been derived by Madan et al. [14]. Savita et al. [16] obtained shearing stresses at a point in anisotropic (monoclinic) elastic layer lying over an irregular monoclinic elastic half-space and gave the generalization of the results obtained in Savita et al. [15]. Both researches resulted that different sizes of rectangular irregularity produced significant variation in shearing stresses for different types of elastic materials.

In this paper, an attempt has been made under the consideration in which a crystal structure having a horizontal orthotropic infinite elastic layer coupling in three different ways ('perfectly welded', 'smooth-rigid' and 'rough-rigid') with an irregular orthotropic elastic half-space to know the deformation due to a very long strike slip fault of finite width situated separately in both elastic mediums of the model. The effect of different sizes of irregularity and variations in fault depth on stresses and displacements has been studied graphically.

2 BASIC EQUATIONS

2.1 Equation of motion

Equations of equilibrium in the Cartesian co-ordinate system (*x,y,z*) for zero body forces are

$$\tau_{ij,j} = 0 \; ; \quad i,j = 1,2,3 \tag{1}$$

where τ_{ij} denotes the stress components. Let (*u, v, w*) denotes the displacement components and e_{ij} represent the strain components then the strain-displacement relations are $e_{11} = \dfrac{\partial u}{\partial x}$, $e_{12} = \dfrac{1}{2}\left(\dfrac{\partial u}{\partial y} + \dfrac{\partial v}{\partial x}\right)$ etc.

From the Generalized Hook's Law, the stress-strain relations for an orthotropic elastic medium in Cartesian co-ordinate system are given by

$$\left.\begin{aligned}\tau_{xx} &= c_{11}e_{xx} + c_{12}e_{yy} + c_{13}e_{zz}\\ \tau_{yy} &= c_{12}e_{xx} + c_{22}e_{yy} + c_{23}e_{zz}\\ \tau_{zz} &= c_{13}e_{xx} + c_{23}e_{yy} + c_{33}e_{zz}\\ \tau_{xy} &= 2c_{66}e_{xy}\\ \tau_{yz} &= 2c_{44}e_{yz}\\ \tau_{zx} &= 2c_{55}e_{zx}\end{aligned}\right\} \tag{2}$$

We consider an elastic medium of anti-plane strain deformation in the *yz*-plane in which the displacement vector is parallel to *x*-axis. For anti-plane strain deformation, the non-zero displacement and stresses are

$$u = u(y,z), \tau_{xz} = c\alpha^2 \frac{\partial u}{\partial z}, \tau_{xy} = c\frac{\partial u}{\partial y} \tag{3}$$

where $c_{55} = c\alpha^2, c_{66} = c$, and $\alpha, c \in R^+$. In case of isotropic elastic medium $c = \mu, \alpha = 1$. For anti-plane strain deformation, equations of equilibrium in (1) reduce to

$$\frac{\partial^2 u}{\partial y^2} + \alpha^2 \frac{\partial^2 u}{\partial z^2} = 0 \tag{4}$$

2.2 Line-source in an infinite medium

The source condition to be satisfied by the resulting tractions becomes (Garg et al., [4])

$$\phi \tau_{1k} v_k \, d\sigma = F \tag{5}$$

where F is the magnitude of the force (per unit length) acting at the point (ξ_2, ξ_3) in an infinite homogeneous orthotropic elastic medium in the positive *x*-direction, and v_k denotes the direction cosines of the exterior normal. Using the source boundary condition (5), the solution of Eq. (4) becomes (Garg et al., [4]) $u = \frac{-F}{4\pi\alpha c}\log\left(\alpha^2 (y-\xi_2)^2 + (z-\xi_3)^2\right)$ for the displacement parallel to the *x*-axis and at any point (*y,z*) of an orthotropic elastic infinite medium, due to a line source, which is parallel to the x-axis and is passing through the point (ξ_2, ξ_3).

2.3 Single couples (*xy*) *and* **(***xz***)**

At the point (ξ_2, ξ_3), there acts a two-dimensional line source, either a single couple (*xy*) or a single couple **(***xz***)**. These displacements (parallel to the *x*-axis, and due to the line source of a single couple **(***xz***)** or **(***xz***)** can be unified into the following integral:

$$u_0 = \int_0^\infty \left[A_0 \sin k(z-\xi_3) + B_0 \cos k(z-\xi_3)\right] e^{-\alpha k|y-\xi_2|} dk \tag{6}$$

The source coefficients A_0 and B_0 for two dimensional buried sources are given in Table 1.

Table 1
Source coefficients for various seismic sources.

Source	A_0	B_0
Single Couple (xy)	0	$\pm\frac{F_{xy}}{2\pi c}$
Single Couple **(**xz**)**	$\frac{F_{xz}}{2\pi\alpha c}$	0

The upper sign is for $y>\xi_2$ and the lower sign for $y<\xi_2$. F_{xy} and F_{xz} denote the moments of couples (xy) and **(**xz**)** respectively. We shall determine the deformation of the model due to a very long strike slip fault situated either in the layer or in the half-space. We note that the source coefficient B_0 (as shown in Table 1) changes sign with $y>\xi_2, y<\xi_2$. We replace B_0 by B_0^1 for $y<\xi_2$ and $B_0=-B_0^1$ for $y>\xi_2$.

3 FORMULATION OF THE PROBLEM

We consider the Cartesian co-ordinate system (x,y,z). Here, z-axis has been taken horizontally and y-axis vertically downward. An infinite orthotropic elastic layer of thickness 'Y' laying horizontally over an irregular orthotropic elastic half-space. The irregularity is assumed to be rectangular in shape. The origin of Cartesian co-ordinate system (x,y,z) is taken at the upper boundary of the layer. Elastic layer having the region ($0\le y\le Y$) is described as medium I whereas the region $y>Y$ is described as medium II. It is assumed that layer is coupled in three different ways such as 'perfectly welded', 'smooth-rigid' and 'rough-rigid' to an irregular base. We formulate the problem into two cases:

Case I: An infinite strike slip fault of finite width 'L' parallel to x-axis lies completely in orthotropic elastic layer whose upper edge is at a distance 'd' from the upper surface of the layer and inclined with an arbitrary dip angle'θ' to a line parallel to z-axis as shown in Fig. 1(a).

Case II: The fault mentioned above lies in lower half-space at same depth 'd' as shown in Fig. 1(b).

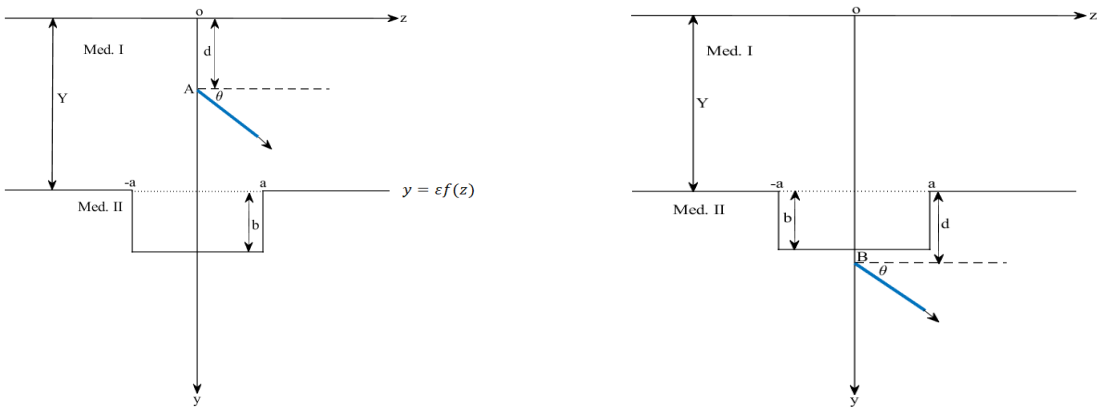

Fig.1
Geometry of an inclined strike-slip fault parallel to the x-axis of finite width L situated in an orthotropic layer (Fig. 1(a)) of uniform thickness Y lying over an irregular orthotropic elastic half-space and secondly situated in irregular orthotropic elastic half-space (Fig. 1(b)); d is the depth of the fault and θ is the dip angle.

Mathematically, the equation of rectangular irregularity having length 2a and depth b is represented as:

$$y=\varepsilon f(z)=\begin{cases} b:|z|\le a \\ 0:|z|>a \end{cases} \tag{7a}$$

where $\varepsilon = \dfrac{b}{2a} \ll 1$ is the perturbation factor. Applying the Fourier Transform technique on Eq. (7a), we obtain

$$f\left(z\right) = sign\left(a - z\right) + sign\left(a + z\right) \tag{7b}$$

The interfacing between the layer and half-space is $y = \varepsilon f\left(z\right)$ and boundary surface $y = 0$ of elastic layer is assumed to be stress free, so the boundary condition at $y = 0$ and interface $y = \varepsilon f\left(z\right)$ is given by

$$\tau_{xy} = 0 \text{ at } y = 0 \tag{8}$$

For perfectly welded contact

$$\begin{aligned} &u^{l}\left(\varepsilon f\left(z\right)\right) = u^{ll}\left(\varepsilon f\left(z\right)\right) \\ &\tau_{xy}^{l}\left(\varepsilon f\left(z\right)\right) - i\,\varepsilon f'\left(z\right)\tau_{xz}^{l}\left(\varepsilon f\left(z\right)\right) = \tau_{xy}^{ll}\left(\varepsilon f\left(z\right)\right) - i\,\varepsilon f'\left(z\right)\tau_{xz}^{ll}\left(\varepsilon f\left(z\right)\right) \end{aligned} \tag{9}$$

For smooth-rigid contact

$$\tau_{xy} = 0 \text{ at } y = \varepsilon f\left(z\right) \tag{10}$$

For rough-rigid contact

$$u = 0 \text{ at } y = \varepsilon f\left(z\right) \tag{11}$$

4 CASE I: WHEN THE LINE-SOURCE LIES IN LAYER

For a line source acting at the point $\left(\xi_2, \xi_3\right)$ of the elastic layer, the expressions for the horizontal displacements in layer and half-space parallel to the line source are obtained by Garg et al. [4]

For $0 \le y \le Y$

$$u^{l} = u_0 + \int_0^{\infty}\left[A_1 \sin k\left(z - \xi_3\right) + B_1 \cos k\left(z - \xi_3\right)\right]e^{-\alpha_1 ky}\,dk + \int_0^{\infty}\left[C_1 \sin k\left(z - \xi_3\right) + D_1 \cos k\left(z - \xi_3\right)\right]e^{\alpha_1 ky}\,dk \tag{12}$$

For $y > Y$

$$u^{ll} = \int_0^{\infty}\left[A_2 \sin k\left(z - \xi_3\right) + B_2 \cos k\left(z - \xi_3\right)\right]e^{-\alpha_2 ky}\,dk \tag{13}$$

The cofficients A_1, A_2, B_1, B_2 etc. For each type of coupling are determined by using the boundary conditions given in Eqs. (8)-(11) as:

$$A_1 = \Delta\left(\left[e^{-k\alpha_1\xi_2} + Te^{k\alpha_1(2\varepsilon f - \xi_2)}\right]A_0 + \frac{i\,\varepsilon f'}{2}\left[B_2 e^{-(\alpha_1+\alpha_2)k\varepsilon f}\left(1 - S'\right)\left(1 - T\right)\right]\right) \tag{14}$$

$$B_1 = \Delta\left(\left[e^{-k\alpha_1\xi_2} + Te^{-k\alpha_1(2\varepsilon f - \xi_2)}\right]B_0^1 - \frac{i\,\varepsilon f'}{2}\left[A_2 e^{-(\alpha_1+\alpha_2)k\varepsilon f}\left(1 - S'\right)\left(1 - T\right)\right]\right) \tag{15}$$

$$C_1 = \Delta\left(\left[e^{-k\alpha_1(2\varepsilon f-\xi_2)} + e^{-k\alpha_1(2\varepsilon f+\xi_2)}\right]TA_0 + \frac{i\varepsilon f'}{2}\left[B_2 e^{-(\alpha_1+\alpha_2)k\varepsilon f}\left(1-S'\right)\left(1-T\right)\right]\right) \tag{16}$$

$$D_1 = \Delta\left(\left[e^{-k\alpha_1(2\varepsilon f+\xi_2)} - e^{-k\alpha_1(2\varepsilon f-\xi_2)}\right]TB_0^1 - \frac{i\varepsilon f'}{2}\left[A_2 e^{-(\alpha_1+\alpha_2)k\varepsilon f}\left(1-S'\right)\left(1-T\right)\right]\right) \tag{17}$$

$$A_2 = \Delta\left(1+T\right)e^{-k(\alpha_1-\alpha_2)\varepsilon f}\begin{bmatrix} e^{-k\alpha_1\xi_2}\left\{A_0 + i\varepsilon f T' B_0^1\right\} \\ +e^{k\alpha_1\xi_2}\left\{A_0 - i\varepsilon f T' B_0^1\right\}\end{bmatrix}\left(1+\left(i\varepsilon f T'\right)^2\right)^{-1} \tag{18}$$

$$B_2 = \Delta\left(1+T\right)e^{-k(\alpha_1-\alpha_2)\varepsilon f}\begin{bmatrix} e^{-k\alpha_1\xi_2}\left\{B_0^1 - i\varepsilon f T' A_0\right\} \\ -e^{k\alpha_1\xi_2}\left\{B_0^1 + i\varepsilon f T' A_0\right\}\end{bmatrix}\left(1+\left(i\varepsilon f T'\right)^2\right)^{-1} \tag{19}$$

where α_1, c_1 and α_2, c_2 are the elastic constants for the Med. I and Med. II, respectively;

$$T = \frac{(s-1)}{(s+1)},\ S = \frac{c_1\alpha_1}{c_2\alpha_2},\ S' = \frac{c_1\alpha_1^2}{c_2\alpha_2^2},\ \Delta^{-1} = \left(1-Te^{-2k\alpha_1\varepsilon f}\right),\ T' = \left(1-S'\right)\left[\left(1-T\right)e^{-k\alpha_1\varepsilon f} + e^{k\alpha_1\varepsilon f}\right]$$

5 CASE II: WHEN THE LINE-SOURCE LIES IN THE HALF-SPACE

For a line source acting at the point (ξ_2, ξ_3) of an irregular elastic half-space, the expressions for the horizontal displacements in layer and half-space parallel to the line source are obtained by Garg et al. [4]

For $0 \le y \le Y$

$$u^I = \int_0^\infty \left[L_1 \sin k\left(z-\xi_3\right) + M_1 \cos k\left(z-\xi_3\right)\right]e^{-\alpha_1 ky}dk + \int_0^\infty \left[P_1 \sin k\left(z-\xi_3\right) + Q_1 \cos k\left(z-\xi_3\right)\right]e^{\alpha_1 ky}dk \tag{20}$$

For $y > Y$

$$u^{II} = u_0 + \int_0^\infty \left[L_2 \sin k\left(z-\xi_3\right) + M_2 \cos k\left(z-\xi_3\right)\right]e^{-\alpha_2 ky}dk \tag{21}$$

The coefficients L_1, L_2, M_1, M_2 etc. for each type of coupling are determined by using the boundary conditions given in Eqs. (8)-(11) and obtained as:

$$L_1 = P_1 = \Delta\left[\left(1-T\right)e^{-k\alpha_1\varepsilon f}e^{k\alpha_2(\varepsilon f-\xi_2)}A_0 - i\varepsilon f'\frac{(S'-1)}{(S+1)}e^{-k\alpha_1\varepsilon f}\left\{B_0^1 e^{k\alpha_2(\varepsilon f-\xi_2)} + M_2 e^{-k\alpha_2\varepsilon f}\right\}\right] \tag{22}$$

$$M_1 = Q_1 = \Delta\left[\left(1-T\right)e^{-k\alpha_1\varepsilon f}e^{k\alpha_2(\varepsilon f-\xi_2)}B_0^1 + i\varepsilon f'\frac{(S'-1)}{(S+1)}e^{-k\alpha_1\varepsilon f}\left\{A_0 e^{k\alpha_2(\varepsilon f-\xi_2)} - L_2 e^{-k\alpha_2\varepsilon f}\right\}\right] \tag{23}$$

$$L_2 = \Delta\left[e^{-2k(\alpha_1-\alpha_2)\varepsilon f}e^{-k\alpha_2\xi_2} - Te^{k\alpha_2(2\varepsilon f-\xi_2)} - 2\alpha_2(S'-1)i\varepsilon f e^{k\alpha_2(2\varepsilon f-\xi_2)}\right]\left(1+2\alpha_2(S'-1)i\varepsilon f'\right)^{-1}A_0 \tag{24}$$

$$M_2 = \Delta\left[e^{-2k(\alpha_1-\alpha_2)\varepsilon f}e^{-k\alpha_2\xi_2} - Te^{k\alpha_2(2\varepsilon f-\xi_2)} + 2\alpha_2(S'-1)i\varepsilon f e^{k\alpha_2(2\varepsilon f-\xi_2)}\right]\left(1+2\alpha_2(S'-1)i\varepsilon f'\right)^{-1}B_0^1 \tag{25}$$

6 INCLINED STRIKE –SLIP FAULT

The displacements in a layered orthotropic elastic half-space due to a very long strike slip line fault of arbitrary inclination θ can be expressed in terms of two different displacement components, one due to horizontal strike slip fault and the other due to a vertical strike slip fault Singh and Garg [5]

$$u = u^{HS}\cos\theta + u^{VS}\sin\theta \tag{26}$$

where u^{HS} and u^{VS} are the displacements for the horizontal and vertical strike slip faults respectively.

The deformation of orthotropic elastic layered medium as a result of a very long inclined strike slip fault situated in the elastic layer (case I) is obtained by using the results obtained by Garg et al. [4]. So, the expressions for the displacements with perfectly welded contact of an elastic layer are obtained by using Eqs. (14)-(19) and (7) in (12)-(13) and from Table 1 as:

For $0 \le y \le Y$

$$u^{I} = \frac{b_0\alpha_1}{2\pi}\left[\begin{array}{l}\sum_{n=0}^{\infty} T^n\left[\dfrac{(2n\varepsilon f + y - \xi_2)\cos\theta - (z-\xi_3)\sin\theta}{(z-\xi_3)^2 + \left[\alpha_1(2n\varepsilon f + y - \xi_2)\right]^2} - \dfrac{(2n\varepsilon f + y + \xi_2)\cos\theta + (z-\xi_3)\sin\theta}{(z-\xi_3)^2 + \left[\alpha_1(2n\varepsilon f + y + \xi_2)\right]^2}\right] \\ +\sum_{n=1}^{\infty} T^n\left[\dfrac{(2n\varepsilon f - y - \xi_2)\cos\theta - (z-\xi_3)\sin\theta}{(z-\xi_3)^2 + \left[\alpha_1(2n\varepsilon f - y - \xi_2)\right]^2} - \dfrac{(2n\varepsilon f - y + \xi_2)\cos\theta + (z-\xi_3)\sin\theta}{(z-\xi_3)^2 + \left[\alpha_1(2n\varepsilon f - y + \xi_2)\right]^2}\right]\end{array}\right] \tag{27a}$$

For $y > Y$

$$u^{II} = \frac{b_0(1+T)}{2\pi}\left[\sum_{n=0}^{\infty} T^n\left[\begin{array}{l}\dfrac{\left[\alpha_1\left((2n+1)\varepsilon f + \xi_2\right) + \alpha_2(y - \varepsilon f)\right]\cos\theta + \alpha_1(z-\xi_3)\sin\theta}{(z-\xi_3)^2 + \left[\alpha_1\left((2n+1)\varepsilon f + \xi_2\right) + \alpha_2(y-\varepsilon f)\right]^2} \\ -\dfrac{\left[\alpha_1\left((2n+1)\varepsilon f - \xi_2\right) + \alpha_2(y - \varepsilon f)\right]\cos\theta - \alpha_1(z-\xi_3)\sin\theta}{(z-\xi_3)^2 + \left[\alpha_1\left((2n+1)\varepsilon f - \xi_2\right) + \alpha_2(y-\varepsilon f)\right]^2}\end{array}\right]ds\right] \tag{27b}$$

The deformation of orthotropic elastic layered medium as a result of a very long inclined strike slip fault situated in the lower half-space (case II) is obtained by using the results obtained by Garg et al. [4]. So, the expressions for the displacements with perfectly welded contact of irregular elastic half-space are obtained by using Eqs. (22)-(25) and (7) in (20)-(21) and from Table 1 as:

For $0 \le y \le Y$

$$u^{I} = \frac{-b_0(1+T)}{2\pi}\left[\sum_{n=0}^{\infty} T^n\left[\begin{array}{l}\dfrac{\left[\alpha_1\left((2n+1)\varepsilon f + y\right) + \alpha_2(\xi_2 - \varepsilon f)\right]\cos\theta + \alpha_2(z-\xi_3)\sin\theta}{(z-\xi_3)^2 + \left[\alpha_1\left((2n+1)\varepsilon f + y\right) + \alpha_2(\xi_2-\varepsilon f)\right]^2} \\ +\dfrac{\left[\alpha_1\left((2n-1)\varepsilon f - y\right) + \alpha_2(\xi_2 - \varepsilon f)\right]\cos\theta + \alpha_2(z-\xi_3)\sin\theta}{(z-\xi_3)^2 + \left[\alpha_1\left((2n-1)\varepsilon f - \xi_2\right)y + \alpha_2(\xi_2-\varepsilon f)\right]^2}\end{array}\right]ds\right] \tag{28a}$$

For $y > Y$

$$u^{II} = \frac{-b_0\alpha_2}{2\pi}\left[\begin{array}{l}\dfrac{(1-T)^2}{\alpha_2}\sum_{n=0}^{\infty} T^n\left[\dfrac{\left[2\alpha_1(n+1)\varepsilon f - \alpha_2(2\varepsilon f - y - \xi_2)\right]\cos\theta + \alpha_2(z-\xi_3)\sin\theta}{\left[2\alpha_1(n+1)\varepsilon f - \alpha_2(2\varepsilon f - y - \xi_2)\right]^2 + (z-\xi_3)^2}\right] \\ -\left[\dfrac{(y-\xi_2)\cos\theta - (z-\xi_3)\sin\theta}{\alpha_2^2(y-\xi_2)^2 + (z-\xi_3)^2} - T\,\dfrac{(2\varepsilon f - y - \xi_2)\cos\theta + (z-\xi_3)\sin\theta}{\alpha_2^2(2\varepsilon f - y - \xi_2)^2 + (z-\xi_3)^2}\right]\end{array}\right]ds \tag{28b}$$

where 'b_0' is the uniform slip; 'ds' is the infinitesimal width of the line dislocation and 's' denote distance from the upper edge of the fault measured in the down-dip direction.

7 PERFECTLY WELDED CONTACT

Putting $\xi_3 = s\cos\theta, \xi_2 = d + s\sin\theta$ into Eq. (27a, 27b) and integrating w.r.t 's' from 0 to L, the expressions for displacement and stresses in welded contact for case I as:

For $0 \le y \le Y$

$$u^{I} = \frac{b_0}{2\pi}\left[\sum_{n=0}^{\infty} T^{n}\left\{\tan^{-1}\frac{T_2}{T_1} - \tan^{-1}\frac{T_4}{T_3}\right\} + \sum_{n=1}^{\infty} T^{n}\left\{\tan^{-1}\frac{T_6}{T_5} - \tan^{-1}\frac{T_8}{T_7}\right\}\right]_0^L \tag{29}$$

$$\tau_{xz}^{I} = \frac{b_0 c_1 \alpha_1^2 T_0}{2\pi}\left[\begin{array}{l}\sum_{n=0}^{\infty} T^{n}\left\{\frac{2n\varepsilon f + y + d + s\sin\theta}{T_3^2 + T_4^2} - \frac{2n\varepsilon f + y - d - s\sin\theta}{T_1^2 + T_2^2}\right\} \\ + \sum_{n=1}^{\infty} T^{n}\left\{\frac{2n\varepsilon f - y + d + s\sin\theta}{T_7^2 + T_8^2} - \frac{2n\varepsilon f - y - d - s\sin\theta}{T_5^2 + T_6^2}\right\}\end{array}\right]_0^L \tag{30}$$

$$\tau_{xy}^{I} = \frac{b_0 c_1 \alpha_1 T_0}{2\pi}\left[\sum_{n=0}^{\infty} T^{n}\left\{\frac{z - s\cos\theta}{T_1^2 + T_1^2} - \frac{z - s\cos\theta}{T_3^2 + T_4^2}\right\} - \sum_{n=1}^{\infty} T^{n}\left\{\frac{z - s\cos\theta}{T_5^2 + T_6^2} - \frac{z - s\cos\theta}{T_7^2 + T_8^2}\right\}\right]_0^L \tag{31}$$

For $y > Y$

$$u^{II} = -\frac{b_0}{2\pi}\sum_{n=0}^{\infty}(1+T)T^{n}\left\{\tan^{-1}\frac{T_{10}}{T_9} + \tan^{-1}\frac{T_{12}}{T_{11}}\right\}_0^L \tag{32}$$

$$\tau_{xz}^{II} = \frac{b_0 c_2 \alpha_2^2 T_0}{2\pi}\left[\sum_{n=0}^{\infty}(1+T)T^{n}\left[\begin{array}{l}\frac{\alpha_1\left((2n+1)\varepsilon f + d\right) + \alpha_2\left(y - \varepsilon f\right) + \alpha_1 s\sin\theta}{T_9^2 + T_{10}^2} \\ -\frac{\alpha_1\left((2n+1)\varepsilon f + d\right) + \alpha_2\left(y - \varepsilon f\right) - \alpha_1 s\sin\theta}{T_{11}^2 + T_{12}^2}\end{array}\right]\right]_0^L \tag{33}$$

$$\tau_{xy}^{II} = \frac{b_0 c_2 \alpha_2 T_0}{2\pi}\left[\sum_{n=0}^{\infty}(1+T)T^{n}\left\{\frac{z - s\cos\theta}{T_{11}^2 + T_{12}^2} - \frac{z - s\cos\theta}{T_9^2 + T_{10}^2}\right\}\right]_0^L \tag{34}$$

Putting $\xi_3 = s\cos\theta, \xi_2 = d + s\sin\theta$ into Eq. (28a, 28b) and integrating w.r.t 's' from 0 to L, we obtain the expressions for displacement and stresses in welded contact for case II as:

For $0 \le y \le Y$

$$u^{I} = -\frac{b_0}{2\pi}\left[\sum_{n=0}^{\infty}(1-T)T^{n}\left[\tan^{-1}\frac{T_{14}}{T_{13}} + \tan^{-1}\frac{T_{16}}{T_{15}}\right]\right]_0^L \tag{35}$$

$$\tau_{xz}^{I}=\frac{b_0c_1\alpha_2^2T_0}{2\pi}\left[\sum_{n=0}^{\infty}(1-T)T^n\left[\begin{array}{l}\dfrac{s\alpha_2\sin\theta+\left[\alpha_1\left((2n+1)\varepsilon f+y\right)-\alpha_2\left(\varepsilon f-d\right)\right]}{T_{13}^2+T_{14}^2}\\+\dfrac{s\alpha_2\sin\theta+\left[\alpha_1\left((2n+1)\varepsilon f-y\right)-\alpha_2\left(\varepsilon f-d\right)\right]}{T_{15}^2+T_{16}^2}\end{array}\right]\right]_0^L \tag{36}$$

$$\tau_{xy}^{I}=-\frac{b_0c_1\alpha_1T_0}{2\pi}\left[\sum_{n=0}^{\infty}(1-T)T^n\left[\frac{z-s\cos\theta}{T_{13}^2+T_{14}^2}-\frac{z-s\cos\theta}{T_{15}^2+T_{16}^2}\right]\right]_0^L \tag{37}$$

For $y>Y$

$$u^{II}=-\frac{b_0}{2\pi}\left[\left[\tan^{-1}\frac{T_{18}}{T_{17}}-T\tan^{-1}\frac{T_{20}}{T_{19}}\right]+\left(1-T^2\right)\sum_{n=0}^{\infty}\tan^{-1}\frac{T_{22}}{T_{21}}\right]_0^L \tag{38}$$

$$\tau_{xz}^{II}=-\frac{b_0c_1\alpha_2^2T_0}{2\pi}\left[\begin{array}{l}\dfrac{\left[\alpha_2\left(y-d-s\sin\theta\right)\right]}{T_{17}^2+T_{18}^2}-T\dfrac{\left[\alpha_2\left[\left(2\varepsilon f-y+d\right)-s\sin\theta\right]\right]}{T_{19}^2+T_{20}^2}\\-\left(1-T^2\right)\sum_{n=0}^{\infty}T^n\dfrac{\left[\alpha_2 s\sin\theta+\alpha_2\left[\left(2n+1\right)\varepsilon f-\left(2\varepsilon f-y+d\right)\right]\right]}{T_{21}^2+T_{22}^2}\end{array}\right]_0^L \tag{39}$$

$$\tau_{xy}^{II}=-\frac{b_0c_1\alpha_2T_0}{2\pi}\left[\frac{z-s\cos\theta}{T_{17}^2+T_{18}^2}-T\frac{z-s\cos\theta}{T_{19}^2+T_{20}^2}+\left(1-T^2\right)\sum_{n=0}^{\infty}T^n\left[\frac{z-s\cos\theta}{T_{21}^2+T_{22}^2}\right]\right]_0^L \tag{40}$$

$$f\left(s\right)\Big|_0^L=f\left(L\right)-f\left(0\right) \tag{41}$$

8 SMOTH-RIGID CONTACT

When the interface between layer and half-space at $y=\varepsilon f\left(z\right)$ is smooth-rigid, without loss of generality, we put $m=0$, i.e $T=1$ in Eqs. (29)-(34). The expressions for displacements and stresses in smooth-rigid contact for case I as:

For $0\le y\le Y$

$$u^{I}=\frac{b_0}{2\pi}\left[\sum_{n=0}^{\infty}\left\{\tan^{-1}\frac{T_2}{T_1}-\tan^{-1}\frac{T_4}{T_3}\right\}+\sum_{n=1}^{\infty}\left\{\tan^{-1}\frac{T_6}{T_5}-\tan^{-1}\frac{T_8}{T_7}\right\}\right]_0^L \tag{42}$$

$$\tau_{xz}^{I}=\frac{b_0c_1\alpha_1^2T_0}{2\pi}\left[\begin{array}{l}\displaystyle\sum_{n=0}^{\infty}\left\{\frac{2n\varepsilon f+y+d+s\sin\theta}{T_3^2+T_4^2}-\frac{2n\varepsilon f+y-d-s\sin\theta}{T_1^2+T_2^2}\right\}\\+\displaystyle\sum_{n=1}^{\infty}\left\{\frac{2n\varepsilon f-y+d+s\sin\theta}{T_7^2+T_8^2}-\frac{2n\varepsilon f-y-d-s\sin\theta}{T_5^2+T_6^2}\right\}\end{array}\right]_0^L \tag{43}$$

$$\tau_{xy}^{I}=\frac{b_0c_1\alpha_1T_0}{2\pi}\left[\sum_{n=0}^{\infty}\left\{\frac{z-s\cos\theta}{T_1^2+T_2^2}-\frac{z-s\cos\theta}{T_3^2+T_4^2}\right\}-\sum_{n=1}^{\infty}\left\{\frac{z-s\cos\theta}{T_5^2+T_6^2}-\frac{z-s\cos\theta}{T_7^2+T_8^2}\right\}\right]_0^L \tag{44}$$

For $y>Y$

$$u^{II}=-\frac{b_0}{\pi}\left[\sum_{n=0}^{\infty}\tan^{-1}\frac{T_{10}}{T_9}+\tan^{-1}\frac{T_{12}}{T_{11}}\right]\Bigg|_0^L \tag{45}$$

$$\tau_{xz}^{II}=\frac{b_0c_2\alpha_2^2T_0}{\pi}\left[\sum_{n=0}^{\infty}\left[\frac{\alpha_1\left((2n+1)\varepsilon f+d\right)+\alpha_2\left(y-\varepsilon f\right)+\alpha_1 s\sin\theta}{T_9^2+T_{10}^2}\right.\right.$$
$$\left.\left.-\frac{\alpha_1\left((2n+1)\varepsilon f-d\right)+\alpha_2\left(y-\varepsilon f\right)-\alpha_1 s\sin\theta}{T_{11}^2+T_{12}^2}\right]\right]\Bigg|_0^L \tag{46}$$

$$\tau_{xy}^{II}=\frac{b_0c_2\alpha_2T_0}{\pi}\left[\sum_{n=0}^{\infty}\left\{\frac{z-s\cos\theta}{T_{11}^2+T_{12}^2}-\frac{z-s\cos\theta}{T_9^2+T_{10}^2}\right\}\right]\Bigg|_0^L \tag{47}$$

Simillarly, without loss of generality we put $m=0$, i.e $T=1$ in Eqs. (35)-(40) to obtain the expressions for displacements and stresses in smooth-rigid contact for case II as:

For $0\le y\le Y$

$$u^{I}=\tau_{xz}^{I}=\tau_{xy}^{I}=0 \tag{48}$$

For $y>Y$

$$u^{II}=-\frac{b_0}{2\pi}\left[\tan^{-1}\frac{T_{18}}{T_{17}}-\tan^{-1}\frac{T_{20}}{T_{19}}\right]\Bigg|_0^L \tag{49}$$

$$\tau_{xz}^{II}=-\frac{b_0c_1\alpha_2^2T_0}{2\pi}\left[\frac{\left[\alpha_2\left(y-d-s\sin\theta\right)\right]}{T_{17}^2+T_{18}^2}-\frac{\left[\alpha_2\left[\left(2\varepsilon f-y+d\right)-s\sin\theta\right]\right]}{T_{19}^2+T_{20}^2}\right]\Bigg|_0^L \tag{50}$$

$$\tau_{xy}^{II}=-\frac{b_0c_1\alpha_2T_0}{2\pi}\left[\frac{z-s\cos\theta}{T_{17}^2+T_{18}^2}-\frac{z-s\cos\theta}{T_{19}^2+T_{20}^2}\right] \tag{51}$$

9 ROUGH –RIGID CONTACT

When the interface between the plate and half-space at $y=\varepsilon f\left(z\right)$ is rough-rigid, without loss of generality, we assume $m\to\infty$, i.e $T=-1$ for putting in Eqs. (29)-(34) to obtain the expressions for displacements and stresses in rough-rigid contact for case I as:

For $0\le y\le Y$

$$u^{I}=\frac{b_0}{2\pi}\left[\sum_{n=0}^{\infty}(-1)^n\left\{\tan^{-1}\frac{T_2}{T_1}-\tan^{-1}\frac{T_4}{T_3}\right\}+\sum_{n=1}^{\infty}(-1)^n\left\{\tan^{-1}\frac{T_6}{T_5}-\tan^{-1}\frac{T_8}{T_7}\right\}\right]\Bigg|_0^L \tag{52}$$

$$\tau_{xz}^{I} = \frac{b_0 c_1 \alpha_1^2 T_0}{2\pi}\left[\begin{bmatrix}\sum_{n=0}^{\infty}(-1)^n\left\{\frac{2n\varepsilon f + y + d + s\sin\theta}{T_3^2+T_4^2} - \frac{2n\varepsilon f + y - d - s\sin\theta}{T_1^2+T_2^2}\right\}\\ \sum_{n=1}^{\infty}(-1)^n\left\{\frac{2n\varepsilon f - y + d + s\sin\theta}{T_7^2+T_8^2} - \frac{2n\varepsilon f - y - d - s\sin\theta}{T_5^2+T_6^2}\right\}\end{bmatrix}\right]_0^L \tag{53}$$

$$\tau_{xy}^{I} = \frac{b_0 c_1 \alpha_1 T_0}{2\pi}\left[\sum_{n=0}^{\infty}(-1)^n\left\{\frac{z - s\cos\theta}{T_1^2+T_2^2} - \frac{z - s\cos\theta}{T_3^2+T_4^2}\right\} - \sum_{n=1}^{\infty}(-1)^n\left\{\frac{z - s\cos\theta}{T_5^2+T_6^2} - \frac{z - s\cos\theta}{T_7^2+T_8^2}\right\}\right]_0^L \tag{54}$$

For $y > Y$

$$u^{II} = \tau_{xz}^{II} = \tau_{xy}^{II} = 0 \tag{55}$$

Simillarly, we assume $m \to \infty$, i.e $T = -1$ for putting in Eqs. (35)-(40) to obtain the expressions for displacements and stresses in rough-rigid contact for case II as:

For $0 \le y \le Y$

$$u^{I} = -\frac{b_0}{\pi}\left[\sum_{n=0}^{\infty}(-1)^n\left[\tan^{-1}\frac{T_{14}}{T_{13}} + \tan^{-1}\frac{T_{16}}{T_{15}}\right]\right]_0^L \tag{56}$$

$$\tau_{xz}^{I} = \frac{b_0 c_1 \alpha_1^2 T_0}{\pi}\left[\sum_{n=0}^{\infty}(-1)^n\left[\begin{matrix}\frac{s\alpha_2\sin\theta + \left[\alpha_1\left((2n+1)\varepsilon f + y\right) - \alpha_2\left(\varepsilon f - d\right)\right]}{T_{13}^2+T_{14}^2}\\ + \frac{s\alpha_2\sin\theta + \left[\alpha_1\left((2n+1)\varepsilon f - y\right) - \alpha_2\left(\varepsilon f - d\right)\right]}{T_{15}^2+T_{16}^2}\end{matrix}\right]\right]_0^L \tag{57}$$

$$\tau_{xy}^{I} = -\frac{b_0 c_1 \alpha_1 T_0}{\pi}\left[\sum_{n=0}^{\infty}(-1)^n\left[\frac{z - s\cos\theta}{T_{13}^2+T_{14}^2} - \frac{z - s\cos\theta}{T_{15}^2+T_{16}^2}\right]\right]_0^L \tag{58}$$

For $y > Y$

$$u^{II} = -\frac{b_0}{2\pi}\left[\sum_{n=0}^{\infty}\left[\tan^{-1}\frac{T_{18}}{T_{17}} + T\tan^{-1}\frac{T_{20}}{T_{19}}\right]\right]_0^L \tag{59}$$

$$\tau_{xz}^{II} = -\frac{b_0 c_1 \alpha_2^2 T_0}{2\pi}\left[\frac{\left[\alpha_2\left(y - d - s\sin\theta\right)\right]}{T_{17}^2+T_{18}^2} + \frac{\left[\alpha_2\left[\left(2\varepsilon f - y + d\right) - s\sin\theta\right]\right]}{T_{19}^2+T_{20}^2}\right]_0^L \tag{60}$$

$$\tau_{xy}^{II} = -\frac{b_0 c_1 \alpha_2^2 T_0}{2\pi}\left[\frac{z - s\cos\theta}{T_{17}^2+T_{18}^2} + \frac{z - s\cos\theta}{T_{19}^2+T_{20}^2}\right]_0^L \tag{61}$$

10 SPECIAL CASE

Putting $\alpha_1 = \alpha_2 = \alpha, c_1 = c_2 = c$, i.e $T = 0$ and absence of irregularity (i.e $b = 0$) in sets of Eqs. (29)-(31) or (32)-(34) i.e deformation field due to Fig. 1(a), we get following expressions for displacements and stresses due to a very

long blind strike-slip fault of finite width 'L' of a uniform orthotropic elastic half-space that coincide with the results obtained by Garg et al. [4].

$$u=\frac{b_0}{2\pi}\left[\tan^{-1}\frac{T_0 s-\left[\alpha^2\left(y-d\right)\sin\theta+z\cos\theta\right]}{\alpha\left[\left(y-d\right)\cos\theta-z\sin\theta\right]}-\tan^{-1}\frac{T_0 s+\left[\alpha^2\left(y+d\right)\sin\theta-z\cos\theta\right]}{\alpha\left[\left(y+d\right)\cos\theta+z\sin\theta\right]}\right] \tag{62}$$

$$\tau_{xz}=\frac{b_0 c\alpha^2 T_0}{2\pi}\left[\begin{array}{c}\dfrac{y+d+s\sin\theta}{\alpha^2\left[z\sin\theta+\left(y+d\right)\cos\theta\right]^2+\left(T_0 s-\left[z\cos\theta-\alpha^2\left(y+d\right)\sin\theta\right]\right)^2}\\ -\dfrac{y-d-s\sin\theta}{\alpha^2\left[z\sin\theta-\left(y-d\right)\cos\theta\right]^2+\left(T_0 s-\left[z\cos\theta+\alpha^2\left(y-d\right)\sin\theta\right]\right)^2}\end{array}\right] \tag{63}$$

$$\tau_{xy}=\frac{b_0 c\alpha T_0}{2\pi}\left[\begin{array}{c}\dfrac{z-s\cos\theta}{\alpha^2\left[z\sin\theta-\left(y-d\right)\cos\theta\right]^2+\left(T_0 s-\left[z\cos\theta+\alpha^2\left(y-d\right)\sin\theta\right]\right)^2}\\ -\dfrac{z-s\cos\theta}{\alpha^2\left[z\sin\theta+\left(y+d\right)\cos\theta\right]^2+\left(T_0 s-\left[z\cos\theta-\alpha^2\left(y+d\right)\sin\theta\right]\right)^2}\end{array}\right] \tag{64}$$

If we make same substitutions $\alpha_1=\alpha_2=\alpha, c_1=c_2=c$, i.e $T=0$ and absence of irregularity, in sets of Eqs. (35)-(37) or (38)-(40), we get same expressions for displacements and stresses obtained in set of Eqs. (62)-(64). Also, it verifies the sanctity of taking two separate models in the present paper shown by Fig. 1(a) and 1(b).

11 NUMERICAL RASULTS

In graphical representation, we examine the effect of variations in depth 'd' of the fault and rectangular irregularity for each type of interfacing condition ('perfectly welded', 'smooth-rigid', 'rough-rigid') due to a uniform slip along a very long strike slip fault of finite width 'L' in both cases (Fig. 1(a), 1(b)). For numerical computation, we use the values of elastic constants used by Chugh et al. [10]. For orthotropic elastic layer $\alpha_1=0.9824$, $c_1=2.87\times10^{11}dynes/cm^2$ or $(28.7GPa)$ for the material baryte and for elastic half-space $\alpha_2=0.9894$, $c_2=8.10\times10^{11}dynes/cm^2$ or $(81GPa)$ for the material olivine. The explicit analytical expressions for displacements and stresses describe the involvement of infinite series appearing at the right hand side of equations (representing displacements and stresses) and converge very rapidly. Therefore, each series truncates after its first twenty terms or each infinite series are replaced by a finite sum of its first twenty terms.

Figs. 2(a)-2(c) represent the variation of the dimensionless surface displacement u^l for orthotropic elastic layer coupling in three different ways i.e. welded contact (WL), smooth-rigid contact (SL) and rough-rigid contact (RL) to an irregular orthotropic elastic half space with dimensionless horizontal distance 'z' at inclination of angle $\theta=15^\circ$ under the hypothesis of Case I. Fig. 2(a, b) and 2(c) represent the variation of surface displacement at a fault depth level $d=0$ and $d=1$ respectively. To compare the effect of irregularity on the displacement component, Figs. 2(b, c) are plotted with assuming irregularity on the interaction boundary surface that couples elastic layer to elastic half space and Fig. 2(a) is plotted in the absence of irregularity. Irregularity, in the lower elastic half-space is of length '$2a$' and depth 'b'. In these figures, we observe that when the fault depth 'd' increases, fluctuations in surface displacement for different types of coupling decrease. Also from these figures, it can be observed that the presence of irregularity makes a significant effect on the displacement component. In Fig. 2(a) we observe that throughout the horizontal distance 'z', surface displacement for rough-rigid interface (RL) lies between surface displacements for smooth-rigid coupling (SL) and welded coupling (WL) while in Figs. 2(b, c) due to the presence of irregularity, (RL) does not lie between (SL) and (WL) on the horizontal distance $-1<z<1$ i.e. on the irregular interface. Moreover Figs. 2(b, c) have discontinuities at points $z=-1$ and $z=1$ of rectangular interaction surface. It is notable that displacement u^l has an additional discontinuity at $z=0$ at the depth $d=1$.

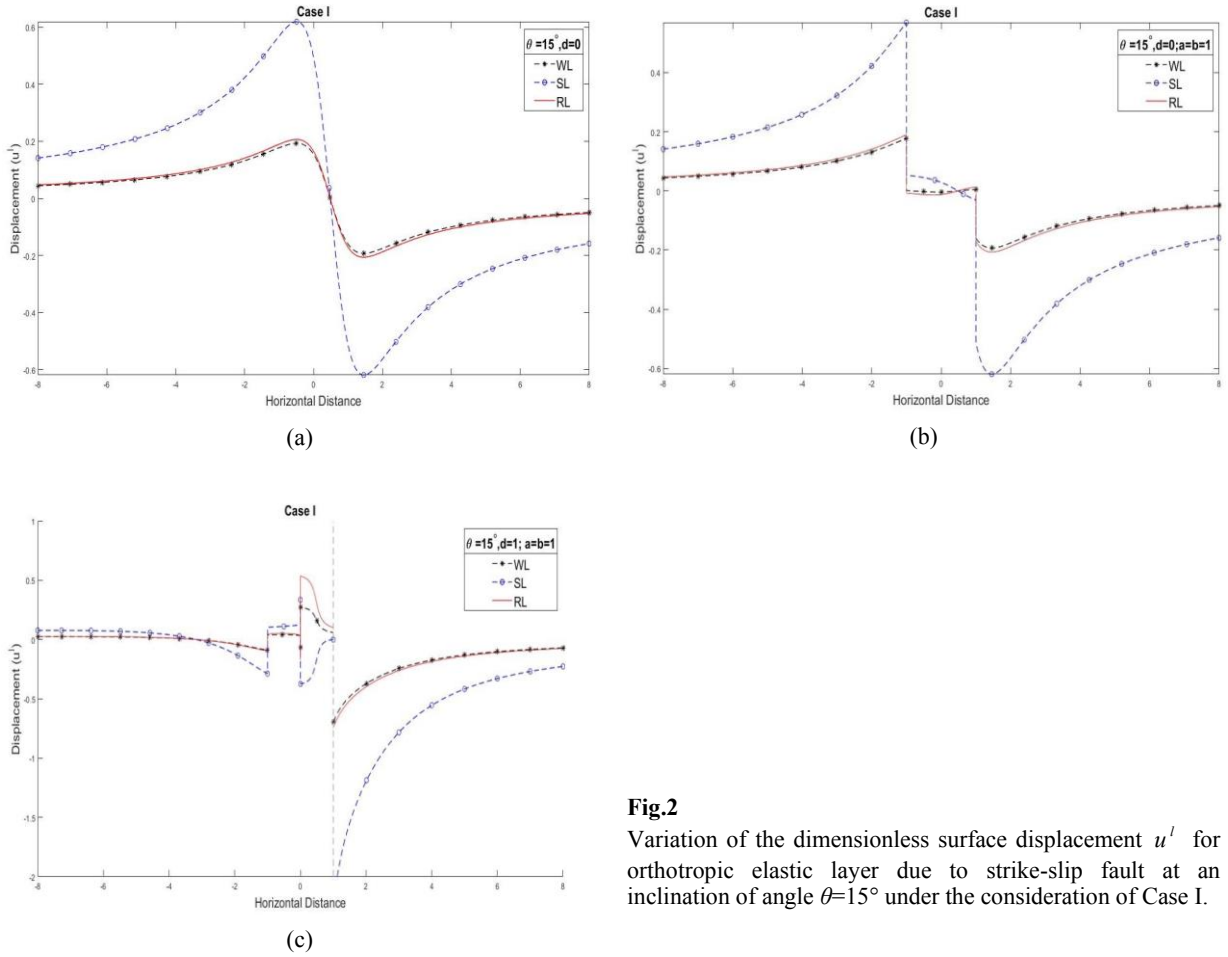

Fig.2
Variation of the dimensionless surface displacement u^{l} for orthotropic elastic layer due to strike-slip fault at an inclination of angle θ=15° under the consideration of Case I.

Figs. 3(a, b) and 4(a, b) represent the variation of the dimensionless shearing stress components τ_{xz}^{l} and τ_{xy}^{l} respectively for orthotropic elastic layer coupling in three different ways welded contact (WL), smooth-rigid contact (SL) and rough-rigid contact (RL) to an irregular orthotropic elastic half space with dimensionless horizontal distance 'z' at inclination of $\theta = 30^{\circ}$ and fault depth level $d = 2$, under the hypothesis of Case I. Figs. 3(a) and 4(a) are plotted by assuming irregularity on the boundary surface connecting layer to half space while Fig. 3(b) and 4(b) are in the absence of irregularity. It is observed that the stress components τ_{xz}^{l} and τ_{xy}^{l} for rough-rigid interface lie between the stresses for perfectly welded and smooth-rigid interfaces in the absence of irregularity while in Figs. 3(a) and 4(a) stress components for welded interfacing condition (WL) lie between the stress components due to (SL) and (RL). Clearly, irregular interface is creating a significant effect on the stresses.

Figs. 5(a)-5(c) represent the variation of the dimensionless surface displacement u^{ll} for irregular orthotropic elastic half-space in welded contact (WH), smooth-rigid contact (SH) and rough-rigid contact (RH) with dimensionless horizontal distance 'z' and inclination $\theta = 15^{\circ}$, under the hypothesis of Case I. Figs. 5(b, c) are obtained in the presence of irregularity having two different dimensionless sizes while Fig. 5(a) is obtained in the absence of irregularity. Figs. 5(b, c) and 5(a) represent the variation of surface displacement at a fault depth level $d = 0.5$ and $d = 1$ respectively. In these figures, it can be noticed that when the fault depth 'd' decreases, magnitudes of the surface displacements for different types of coupling increase. It is also observed that surface displacement u^{ll} of orthotropic elastic half-space in Figs. 5(b, c), are also effected due to the different sizes of irregularity. In Fig. 5(b), it is clear that (SH) and (RH) have three points of discontinuity on the horizontal distance 'z' at $z = -2, 0, 2$ while (WH) has only one point of discontinuity at $z = 0$.

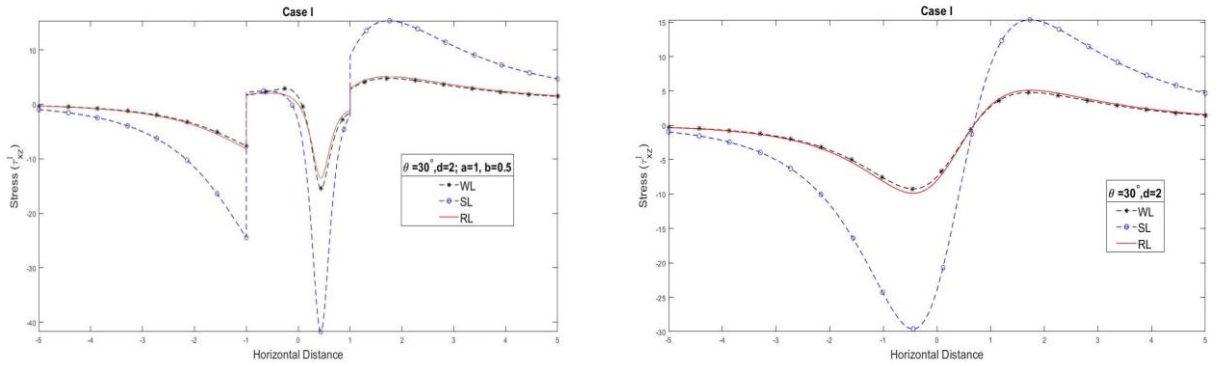

(a) (b)

Fig.3

Variation of the dimensionless surface shearing stress components τ^{l}_{xz} for orthotropic elastic layer due to strike-slip fault at an inclination of angle θ=30° under the consideration of Case I.

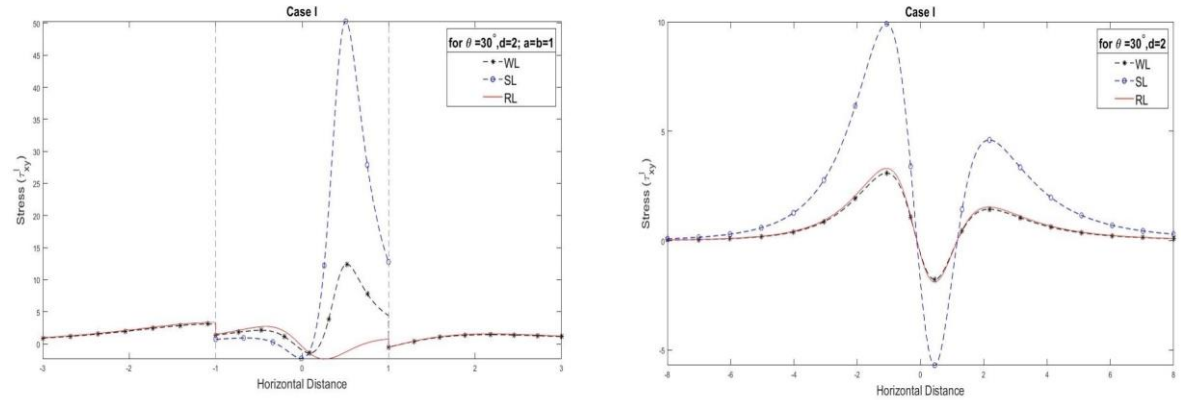

(a) (b)

Fig.4

Variation of the dimensionless surface shearing stress components τ^{l}_{xy} for orthotropic elastic layer due to strike-slip fault at an inclination of angle θ=30° under the consideration of Case I.

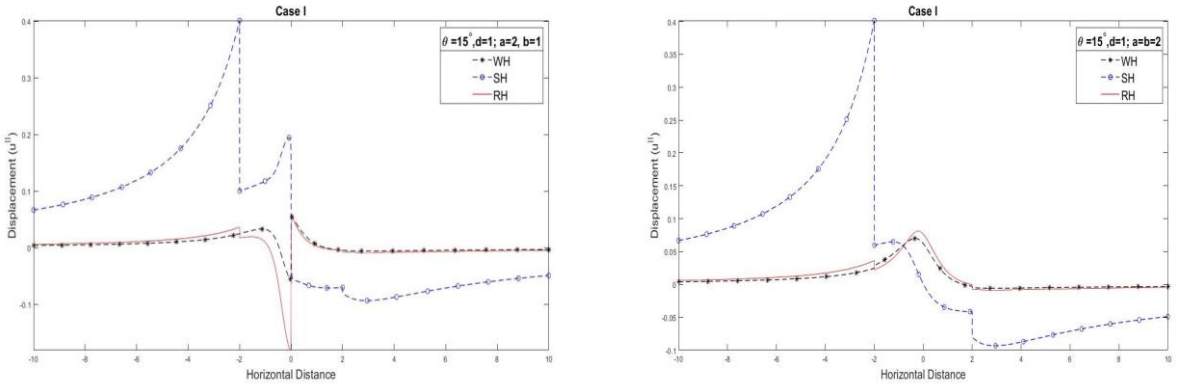

(a) (b)

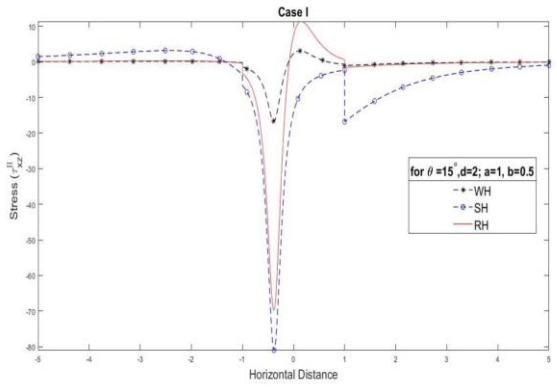

(c)

Fig.5
Variation of the dimensionless surface displacement u^{II} for irregular orthotropic elastic half-space due to strike-slip fault at an inclination of angle θ=15° under the consideration of Case I.

Figs. 6(a, b) and 7(a, b) represent the variation of the dimensionless shearing stress component τ_{xz}^{II} and τ_{xy}^{II} respectively for orthotropic elastic half-space in welded contact (WH), smooth-rigid contact (SH) and rough-rigid contact (RH) with dimensionless horizontal distance 'z' at inclination $\theta = 15^{\circ}$ and fault depth level $d = 2$ and $d = 1$ respectively under the hypothesis of Case I. Figs. 6(a) and 7(a) are plotted by assuming irregularity on the boundary surface connected layer to half space while Fig. 6(b) and 7(b) are in the absence of irregularity. In Figs. 6(b) and 7(b), it is observed that the stress components τ_{xz}^{II} and τ_{xy}^{II} for rough-rigid interface lie between the stresses for perfectly welded and smooth-rigid interfaces while in Fig. 7(a) stress component due to (WH) lies between (SH) and (RH) and also changes its sign on irregular interface $-1<z<1$. In Figs. 6(a) and 7(a), stress components due to different type of couplings (WH), (SH) and (RH) have two points of discontinuity at $z = -1$ and $z = 1$ and make a significant change on irregular surface.

Figs. 8(a)-8(c) exhibit the variation of the surface displacement u^{I} for orthotropic elastic layer in welded contact (WL), smooth-rigid contact (SL) and rough-rigid contact (RL) with dimensionless horizontal distance 'z' and inclination $\theta = 30^{\circ}$ under the hypothesis of Case II. Figs. 8(a) and 8(b, c) represent the variation of surface displacement at a fault depth level $d = 0$ and $d = 1$ respectively. In these figures, we observe that when the fault depth 'd' increases, magnitudes of the surface displacement for different types of coupling increase. From these figures, it is noticed that surface displacement u^{I} for elastic layer due to smooth-rigid contact (SL) is zero throughout the horizontal distance 'z' (Eq. (48)). The surface displacements in Fig. 8(c) are obtained due to an irregular interaction boundary surface while Fig. 8(a, b) are drawn on regular boundary surface. In Fig. 8(c), surface displacements due to welded contact (WL) and rough-rigid contact (RL) have discontinuities at the points $z = -1$ and $z = 1$ and also results in increment in magnitudes in the region $-1<z<1$ due to significant effect of presence of irregularity. In all figures, displacement components for welded interfacing condition (WL) lie between the stress components due to (SL) and (RL).

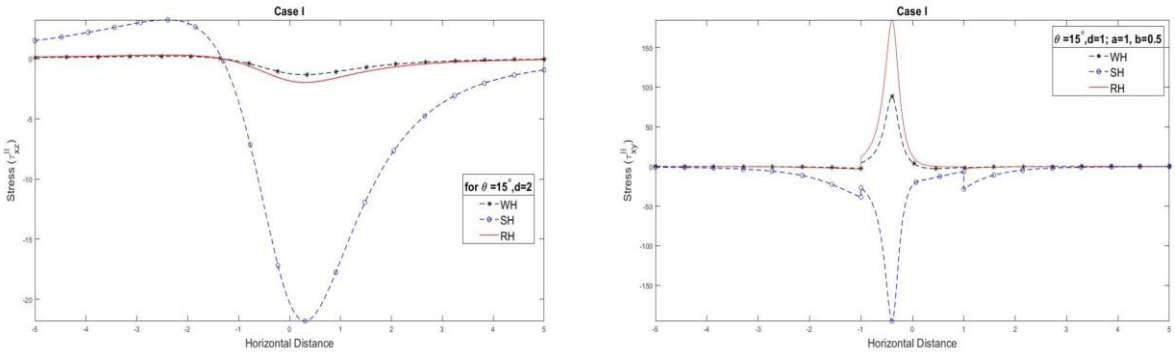

(a) (b)

Fig.6
Variation of the dimensionless surface shearing stress components τ_{xz}^{II} for irregular orthotropic elastic half-space due to strike-slip fault at an inclination of angle θ=15° under the consideration of Case I.

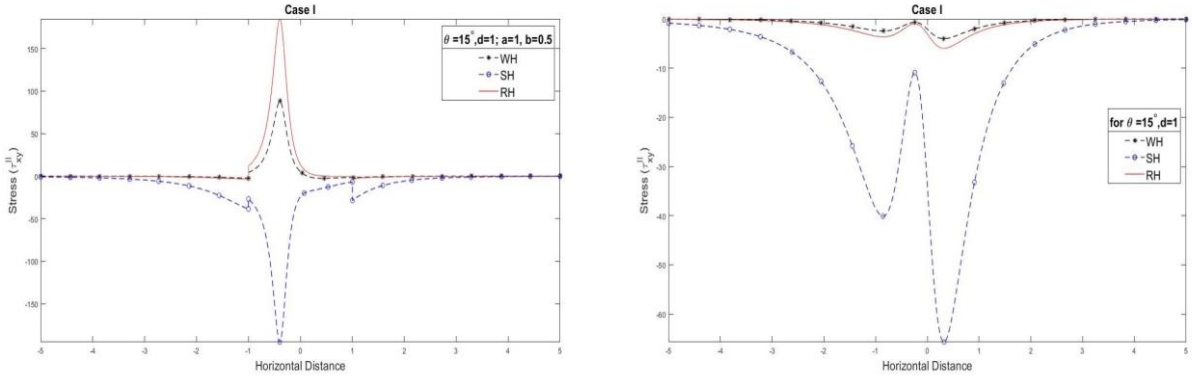

(a) (b)

Fig.7

Variation of the dimensionless surface shearing stress components τ_{xy}^{II} for irregular orthotropic elastic half-space due to strike-slip fault at an inclination of angle θ=15° under the consideration of Case I.

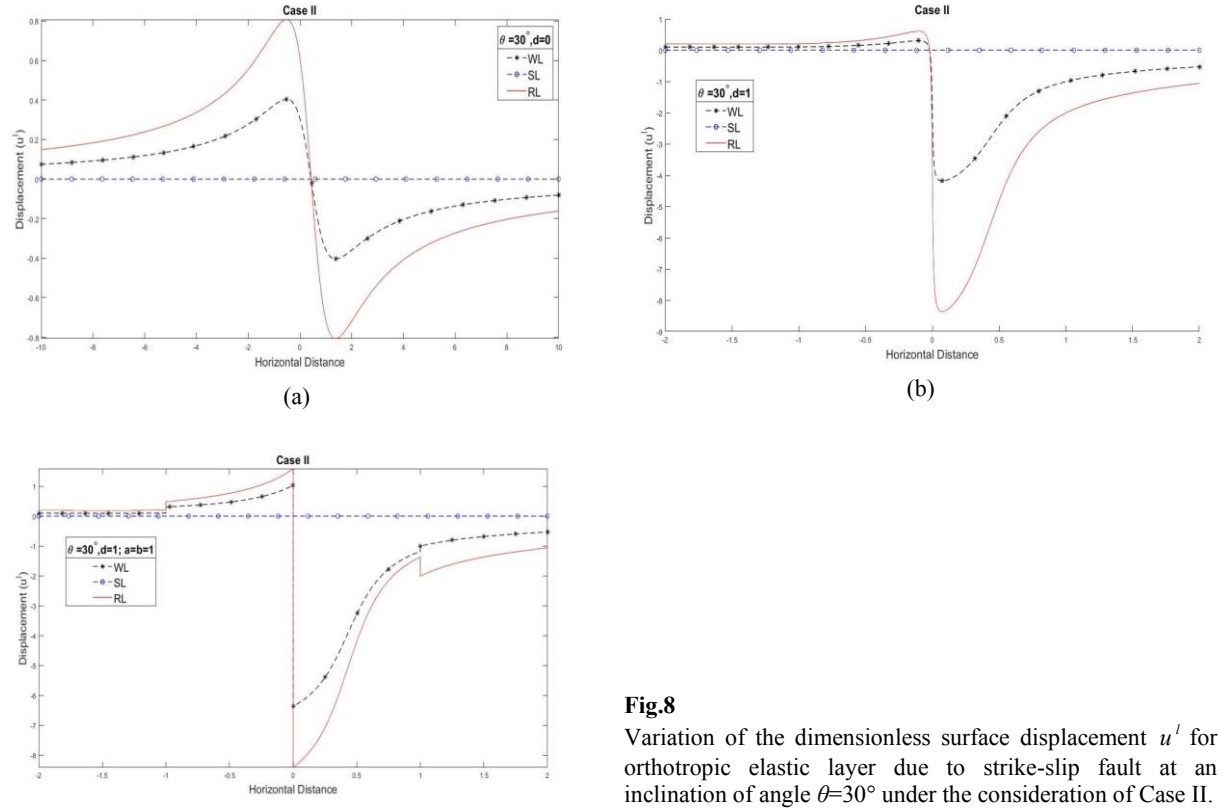

(a) (b)

(c)

Fig.8

Variation of the dimensionless surface displacement u^{l} for orthotropic elastic layer due to strike-slip fault at an inclination of angle θ=30° under the consideration of Case II.

Figs. 9(a, b) and 10(a, b) represent the variation of the dimensionless shearing stress components τ_{xz}^{l} and τ_{xy}^{l} for orthotropic elastic layer in welded contact (WL), smooth-rigid contact (SL) and rough-rigid contact (RL) with dimensionless horizontal distance 'z' and angle $\theta = 15^{\circ}$ at fault depth level $d = 1$ and $d = 2$ respectively, under the hypothesis of Case II. In all figures, stress components τ_{xz}^{l} and τ_{xy}^{l} of elastic layer in smooth-rigid contact (SL) are zero throughout the horizontal distance 'z' (Eq. (48)). The stress components τ_{xz}^{l} and τ_{xy}^{l} in 9(a) and 10(a) are obtained due to irregular boundary surface while Figs. 9(b) and 10(b) are studied on regular boundary surface. Stress components due to rough-rigid contact (RL) and perfectly welded contact (WL) in Figs. 9(b) and 10(b) have two

points of discontinuity at the end points of irregular boundary surface. From Figs. 9(a, b), it is noticed that stress components for (RL) lie between the stress component τ_{xz}^{l} for welded contact (WL) and smooth-rigid contact (SL) throughout the horizontal distance but in Figs. 10(a, b) stress components τ_{xy}^{l} of elastic layer due to welded contact (WL) lie between the stress components of elastic layer due to (RL) and (SL). Clearly, irregular interface is creating a significant effect on the stresses.

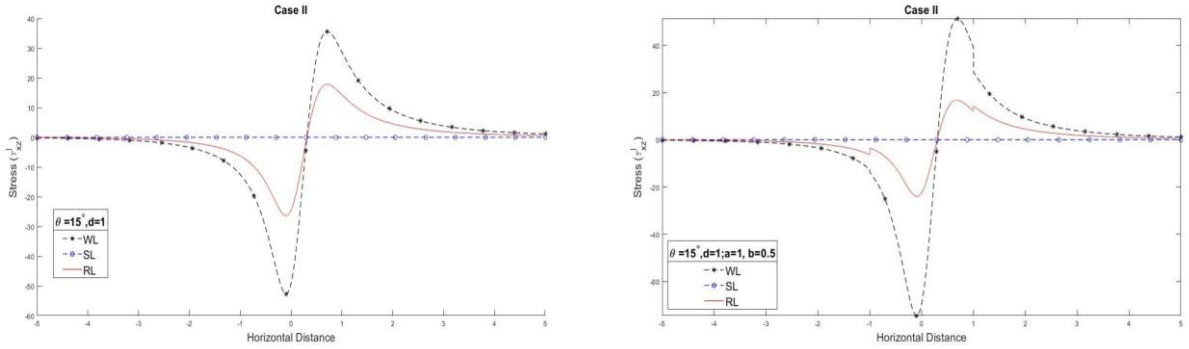

(a) (b)

Fig.9

Variation of the dimensionless surface shearing stress components τ_{xz}^{l} for orthotropic elastic layer due to strike-slip fault at an inclination of angle θ=15° under the consideration of Case II.

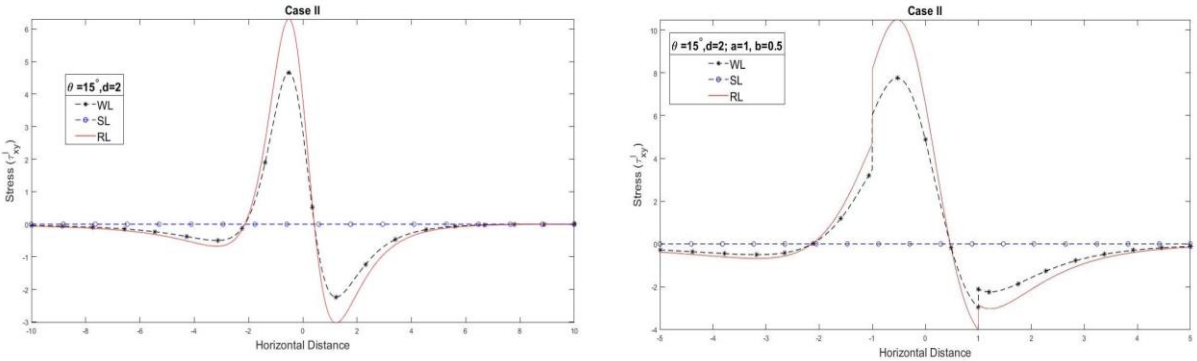

(a) (b)

Fig.10

Variation of the dimensionless surface shearing stress components τ_{xy}^{l} for orthotropic elastic layer due to strike-slip fault at an inclination of angle θ=15° under the consideration of Case II.

Figs. 11(a, b) represent the variation of the dimensionless surface displacement u^{ll} for irregular orthotropic elastic half-space connected with different type of coupling, welded contact (WH), smooth-rigid contact (SH) and rough-rigid contact (RH) with dimensionless horizontal distance 'z' and angle $\theta = 30^{\circ}$ under the hypothesis of Case II. Fig. 11(a) is obtained in the absence of irregularity from the interaction boundary surface of layer to half space and 11(b) is plotted by assuming rectangular irregularity on the interaction boundary surface. We observe that presence of irregularity makes a notable change on the displacement components u^{ll} for each different type of coupling. In Fig. 11(a), surface displacement due to all interfacing conditions having two points that breaks the curves on the horizontal distance 'z'. Presence of irregularity in Fig. 11(b) creates two points of discontinuity at $z = -1$ and $z = 1$.

Figs. 12(a, b) and 13(a, b) represent the variation of dimensionless shearing stress components τ_{xz}^{ll} and τ_{xy}^{ll} respectively for irregular orthotropic elastic half-space welded contact (WH), smooth-rigid contact (SH) and in rough-rigid contact (RH) with the dimensionless horizontal distance 'z' and inclination of angle $\theta = 30^{\circ}$ under the hypothesis of Case II. Figs. 12(a, b) and 13(a, b) are obtained for two different fault depth level $d = 0, 0.5$ and in the

absence of irregularity from the interaction boundary surface of elastic layer and half space. In these figures, we observe that stress components τ_{xz}^{ll} and τ_{xy}^{ll} due to perfectly welded contact (WH) lie between the stress components of elastic half-space due to rough-rigid contact (RH) and smooth-rigid contact (SH). Also the magnitude of stress components τ_{xz}^{ll} and τ_{xy}^{ll} increases with the increase in fault depth '*d*'.

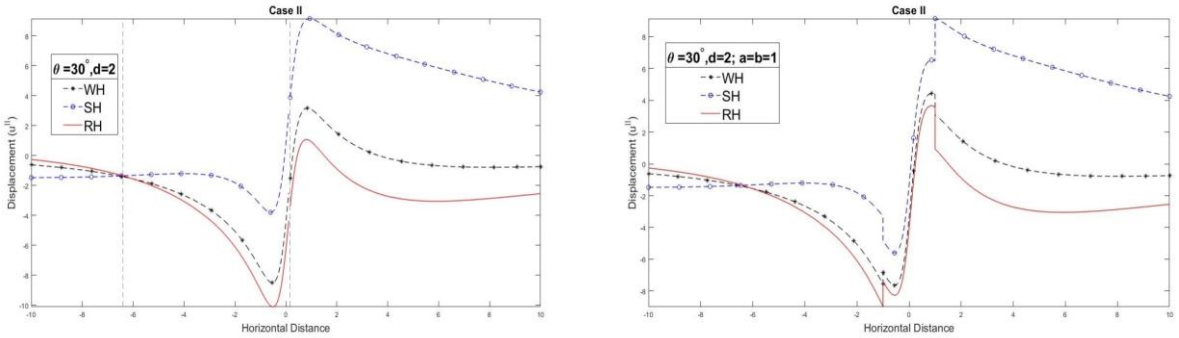

(a) (b)

Fig.11

Variation of the dimensionless surface displacement u^{ll} for irregular orthotropic elastic half-space due to strike-slip fault at an inclination of angle θ=30° under the consideration of Case II.

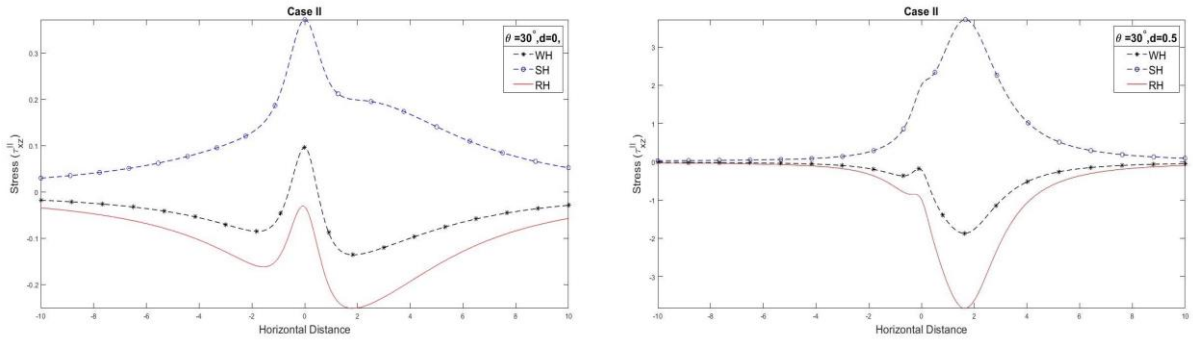

(a) (b)

Fig.12

Variation of the dimensionless surface shearing stress components τ_{xz}^{ll} for irregular orthotropic elastic half-space due to strike-slip fault at an inclination of angle θ=30° under the consideration of Case II.

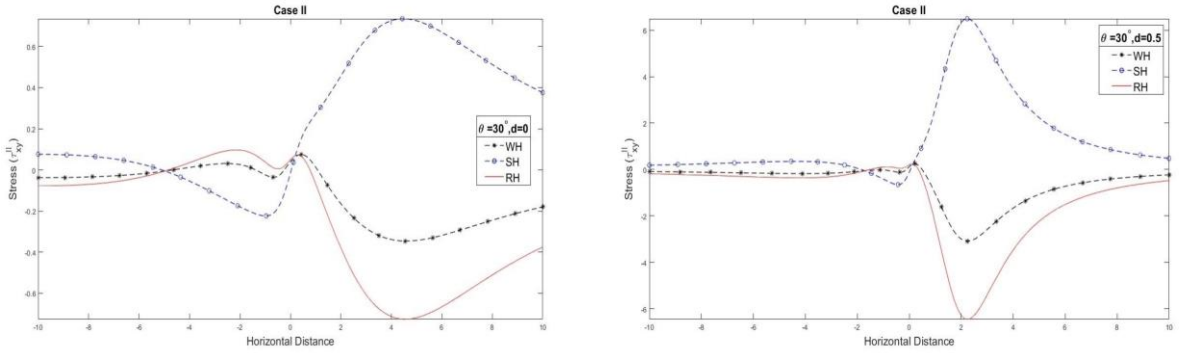

(a) (b)

Fig.13

Variation of the dimensionless surface shearing stress components τ_{xy}^{ll} for irregular orthotropic elastic half-space due to strike-slip fault at an inclination of angle θ=30° under the consideration of Case II.

12 CONCLUSIONS

We have examined the effect of a very long strike slip fault of finite width situated at a distance '*d*' from the surface. Three types of interfaces, 'perfectly welded, smooth-rigid, rough-rigid' have been considered between the elastic layer and irregular half-space. As per our considerations the present work has been explained by dividing into two cases and the consequences of this work are as follows:

1. The results obtained in case first are in addition to the earlier research work of Chugh et al. [10], in the sense that the interface between the layer and half-space may be irregular which is more realistic than regular interfac crustal structure.
2. The results obtained in case second are generalizations of the results obtained by Arya et al. [7], in the sense that the physical structure considered in the present paper is layered irregular anisotropic elastic model.
3. Earthquake on San Andreas Fault occurred at the shallow depths of 20 *km* approximately and extended roughly to 1200 kilometers in strike-slip motions through the California. For such type of shallow earthquakes, the elastic layer of our model may be identified with the topmost brittle region of the earth crust, and the welded interfacing to an elastic half-space with a crustal zone.
4. The Palos Verdes is also a very long strike-slip fault on the south-western edge of the Los Angeles, with its slip in the sediments. Such sedimentary rocks may be identified to an elastic layer consisting almost uniform thickness and the bottom surface of elastic layer may be taken as 'rough-rigid', where the displacements and stresses are zero (Eq. (55)).
5. In engineering mathematics, physical problems dealing with a layer of petroleum material slipping over a base. We observe that a 'smooth-rigid' interfacing condition is applicable between petroleum layer and the base. This interfacing condition is used to determine the effect of lubrication and it has been observed that the vertical displacement vector and shear stress components vanished.

APPENDIX

$$T_0 = \left[\cos^2\theta + \alpha_1^2 \sin^2\theta\right]$$
$$T_1 = \alpha_1\left[\left(2n\varepsilon f + y - d\right)\cos\theta - z\sin\theta\right]$$
$$T_2 = T_0 s - \left[\alpha_1^2\left(2n\varepsilon f + y - d\right)\sin\theta + z\cos\theta\right]$$
$$T_3 = \alpha_1\left[\left(2n\varepsilon f + y + d\right)\cos\theta + z\sin\theta\right]$$
$$T_4 = T_0 s + \left[\alpha_1^2\left(2n\varepsilon f + y + d\right)\sin\theta - z\cos\theta\right]$$
$$T_5 = \alpha_1\left[\left(2n\varepsilon f - y - d\right)\cos\theta - z\sin\theta\right]$$
$$T_6 = T_0 s - \left[\alpha_1^2\left(2n\varepsilon f - y - d\right)\sin\theta + z\cos\theta\right]$$
$$T_7 = \alpha_1\left[\left(2n\varepsilon f - y + d\right)\cos\theta + z\sin\theta\right]$$
$$T_8 = T_0 s + \left[\alpha_1^2\left(2n\varepsilon f - y + d\right)\sin\theta - z\cos\theta\right]$$
$$T_9 = \left[\alpha_1\left(\left(2n+1\right)\varepsilon f + d\right) + \alpha_2\left(y - \varepsilon f\right)\right]\cos\theta + \alpha_1 z\sin\theta$$
$$T_{10} = T_0 s + \left[\alpha_1^2\left(\left(2n+1\right)\varepsilon f + d\right) + \alpha_1\alpha_2\left(y - \varepsilon f\right)\right]\sin\theta - z\cos\theta$$
$$T_{11} = -\left[\alpha_1\left(\left(2n+1\right)\varepsilon f - d\right) + \alpha_2\left(y - \varepsilon f\right)\right]\cos\theta + \alpha_1 z\sin\theta$$
$$T_{12} = T_0 s - \left[\alpha_1^2\left(\left(2n+1\right)\varepsilon f - d\right) + \alpha_1\alpha_2\left(y - \varepsilon f\right)\right]\sin\theta - z\cos\theta$$
$$T_{13} = z\alpha_2\sin\theta + \left[\alpha_1\left(\left(2n+1\right)\varepsilon f + y\right) - \alpha_2\left(\varepsilon f - d\right)\right]\cos\theta$$
$$T_{14} = T_0 s - \left[z\cos\theta - \alpha_2\sin\theta\left[\alpha_1\left(\left(2n+1\right)\varepsilon f + y\right) - \alpha_2\left(\varepsilon f - d\right)\right]\right]$$
$$T_{15} = z\alpha_2\sin\theta + \left[\alpha_1\left(\left(2n+1\right)\varepsilon f - y\right) - \alpha_2\left(\varepsilon f - d\right)\right]\cos\theta$$

$$T_{16} = T_0 s - \left[z \cos\theta - \alpha_2 \sin\theta \left[\alpha_1 \left((2n+1)\varepsilon f - y \right) - \alpha_2 \left(\varepsilon f - d \right) \right] \right]$$

$$T_{17} = \alpha_2 \left(z \sin\theta - \left(y - d \right) \cos\theta \right)$$

$$T_{18} = T_0 s - \left[z \cos\theta + \alpha_2^2 \left(y - d \right) \sin\theta \right]$$

$$T_{19} = \alpha_2 \left(z \sin\theta - \left(2\varepsilon f - y + d \right) \cos\theta \right)$$

$$T_{20} = T_0 s - \left[z \cos\theta + \alpha_2^2 \left(2\varepsilon f - y + d \right) \sin\theta \right]$$

$$T_{21} = z \alpha_2 \sin\theta + \left[2\alpha_1 \left(n+1 \right) \varepsilon f - \alpha_2 \left(2\varepsilon f - y - d \right) \right] \cos\theta$$

$$T_{22} = T_0 s - \left[z \cos\theta - \left[2\alpha_1 \left(n+1 \right) \varepsilon f - \alpha_2 \left(2\varepsilon f - y - d \right) \right] \alpha_2 \sin\theta \right]$$

ACKNOWLEDGMENTS

One of the authors (Savita) is thankful to HRDG Council of Scientific & Industrial Research for sanctioning SRF scholarship. The authors are also thankful to the unknown reviewer for comments and suggestions to enriched our manuscript considerably.

REFERENCES

[1] Crampin S., 1989, Suggestions for a consistent terminology for seismic anisotropy, *Geophysical Prospecting* **37**(7): 753-770.

[2] Singh S. J., Rani S., 1994, Lithospheric deformation associated with two-dimensional strike-slip faulting, *Journal of Physics of the Earth* **42**:197-220.

[3] Rani S., Singh S.J., 1992, Static deformation of two welded half-space due to dip-slip faulting, *Proceedings of the Indian Academy of Sciences - Earth & Planetary Sciences* **101**(3): 269-282.

[4] Garg N.R., Madan D.K., Sharma R.K., 1996, Two dimensional static deformation of an orthotropic elastic medium due to seismic sources, *Physics of the Earth and Planetary Interiors* **94**: 43-62.

[5] Singh S.J., Garg N.R., 1985, On two-dimensional elastic dislocations in a multilayered half-space, *Physics of the Earth and Planetary Interiors* **40**(2): 135-145.

[6] Bonafede M., Parenti B., Rivalta E., 2002, On strike-slip faulting in layered media, *Geophysical Journal International* **149**: 698-723.

[7] Arya P., Madan D.K., Garg N.R., Gaba A., 2016, Shear stress and displacement for strike-slip dislocation in an orthotropic elastic half-space with rigid surface, *International Journal of Applied Science-Research and Review* **2016**: 097-112.

[8] Garg N.R., Sharma R.K., 1992, Deformation of an elastic layer coupling in different ways to a base due to a very long vertical strike-slip dislocation, *Proceedings of the Indian Academy of Sciences-Earth and Planetary Sciences* **101**: 255-268.

[9] Madan D.K., Garg N.R., 1997, Static deformation of an orthotropic horizontal elastic layer coupling in different ways to a base due to a very long inclined strike-slip fault embedded in the layer, *Indian Journal of Pure & Applied Mathematics* **28**(5): 697-712.

[10] Chugh S., Singh K., Madan D.K., 2009, Two-dimensional static deformation of an orthotropic elastic layered half-space due to blind strike-slip fault, *ISET Journal of Earthquake Technology* **46**(2): 109-124.

[11] Malik M., Singh M., 2013, Deformation of a uniform half-space with rigid boundary due to strike-slip line source, *IOSR Journal of Mathematics* **5**: 30-41.

[12] Selim M. M., 2008, Effect of irregularity on static deformation of elastic half-space, *International Journal of Modern Physics* **22**(14): 2241-2253.

[13] Madan D.K., Gaba A., 2016, 2-Dimensional deformation of an irregular orthotropic elastic medium, *IOSR Journal of Mathematics* **12**(4): 101-113.

[14] Madan D.K., Arya P., Garg N.R., Singh K., 2017, Stresses in an orthotropic elastic layer lying over in irregular isotropic elastic half-space, *International Journal of Current Research and Review* **09**(04): 15-20.

[15] Savita., Sahrawat R.K., Malik M., 2021, Stresses in a monoclinic elastic layer lying over an irregular isotropic elastic half-space, *Advances and Applications in Mathematical Sciences* **21**(1): 21-39.

[16] Savita., Sahrawat R.K., Malik M., 2021, Stresses in a monoclinic elastic plate placed upon an irregular mon oclinic elastic half-space, *Indian Journal of Science and Technology* **14**(1): 55-70.